Solar Cells Hot Paper

Zitierweise: *Angew. Chem. Int. Ed.* **2020**, *59*, 9324–9329
Internationale Ausgabe: doi.org/10.1002/anie.202000892
Deutsche Ausgabe: doi.org/10.1002/ange.202000892

Phenanthrene-Fused-Quinoxaline as a Key Building Block for Highly Efficient and Stable Sensitizers in Copper-Electrolyte-Based Dye-Sensitized Solar Cells

Huiyun Jiang[+], Yameng Ren[+], Weiwei Zhang, Yongzhen Wu, Etienne Christophe Socie, Brian Irving Carlsen, Jacques-E. Moser, He Tian, Shaik Mohammed Zakeeruddin, Wei-Hong Zhu, and Michael Grätzel**

Abstract: *Dye-sensitized solar cells (DSSCs) based on $Cu^{II/I}$ bipyridyl or phenanthroline complexes as redox shuttles have achieved very high open-circuit voltages (V_{OC}, more than 1 V). However, their short-circuit photocurrent density (J_{SC}) has remained modest. Increasing the J_{SC} is expected to extend the spectral response of sensitizers to the red or NIR region while maintaining efficient electron injection in the mesoscopic TiO_2 film and fast regeneration by the Cu^{I} complex. Herein, we report two new D-A-π-A-featured sensitizers termed* ***HY63*** *and* ***HY64****, which employ benzothiadiazole (BT) or phenanthrene-fused-quinoxaline (PFQ), respectively, as the auxiliary electron-withdrawing acceptor moiety. Despite their very similar energy levels and absorption onsets,* ***HY64****-based DSSCs outperform their* ***HY63*** *counterparts, achieving a power conversion efficiency (PCE) of 12.5 %. PFQ is superior to BT in reducing charge recombination resulting in the near-quantitative collection of photogenerated charge carriers.*

Copper-complex-based redox shuttles are increasingly being used in dye-sensitized solar cells (DSSCs) since they can reach open-circuit voltages (V_{OC}) over 1.0 V, thereby boosting the power conversion efficiency (PCE).[1–4] Moreover, these $Cu^{II/I}$ bipyridyl or phenanthroline complexes exhibit very low reorganization energies to allow the regeneration of sensitizers to proceed rapidly at low driving force.[5,6] However, the moderate value of short-circuit current densities (J_{SC}) in copper-based DSSCs becomes the bottleneck for further PCE improvement.[7–11] Indeed, the current lack of sensitizers with extended long-wavelength response prevents the full potential of the copper redox shuttles from being exploited.

The well-known **Y123** dye (Figure 1a) is one of the most efficient and widely used sensitizers for copper-based DSSCs. However, it exhibits an undesirably large optical energy gap with a relatively narrow incident photon-to-electron conversion efficiency (IPCE) plateau in the region of 400–600 nm.[12–14] Extending the spectral response towards a longer wavelength is essential to further improve the PCE for copper-based DSSCs. To this effect, the D-A-π-A strategy that incorporates an additional electron-withdrawing group as an auxiliary acceptor to extend the absorption spectra seems to be appropriate as it decreases the HOMO–LUMO energy gap with targeted downshift in both the HOMO and LUMO levels of sensitized dyes.[15–20] There have already been attempts to employ benzothiadiazole (BT) or quinoxaline as the auxiliary acceptors to widen the spectral response of sensitizers for copper-based DSSCs. However, these dyes have not delivered the desired J_{SC} increase.[7,8,21,22]

Herein, we introduce the organic dye **HY64** (Figure 1a) with an electron-withdrawing phenanthrene-fused-quinoxaline (PFQ)[23–25] as the auxiliary acceptor for copper-electrolyte-based DSSCs. It shows a desirably red-shifted absoption onset along with greatly improved photocurrents, as well as delivering a high V_{OC} and fill factor (*FF*), thereby achieving the solar to electric power conversion efficiency (PCE) of 12.5 % under standard AM1.5G sunlight, a record for DSSCs using an organic sensitizer. We find that the **HY64** endowed with a PFQ unit has a much superior J_{SC} and V_{OC} compared to the closely related dye **HY63** (Figure 1a), which features the

[*] H. Jiang,[+] W. Zhang, Prof. Y. Wu, Prof. H. Tian, Prof. W. Zhu
Key Laboratory for Advanced Materials and
Joint International Research Laboratory of Precision Chemistry and Molecular Engineering,
Feringa Nobel Prize Scientist Joint Research Center,
Shanghai Key Laboratory of Functional Materials Chemistry,
Institute of Fine Chemicals,
School of Chemistry and Molecular Engineering,
East China University of Science and Technology
Shanghai 200237 (China)
E-mail: whzhu@ecust.edu.cn

H. Jiang,[+] Dr. Y. Ren,[+] S. M. Zakeeruddin, Prof. M. Grätzel
Laboratory of Photonics and Interfaces,
Institute of Chemical Sciences and Engineering,
École Polytechnique Fédérale de Lausanne (EPFL)
1015 Lausanne (Switzerland)
E-mail: michael.graetzel@epfl.ch

B. I. Carlsen
Laboratory of Photomolecular Science,
Institute of Chemical Sciences and Engineering,
École Polytechnique Fédérale de Lausanne (EPFL) (Switzerland)

E. C. Socie, J.-E. Moser
Photochemical Dynamics Group,
Institute of Chemical Sciences and Engineering,
École Polytechnique Fédérale de Lausanne (EPFL) (Switzerland)

[+] These authors contributed equally to this work.

Supporting information and the ORCID identification number(s) for the author(s) of this article can be found under: https://doi.org/10.1002/anie.202000892.

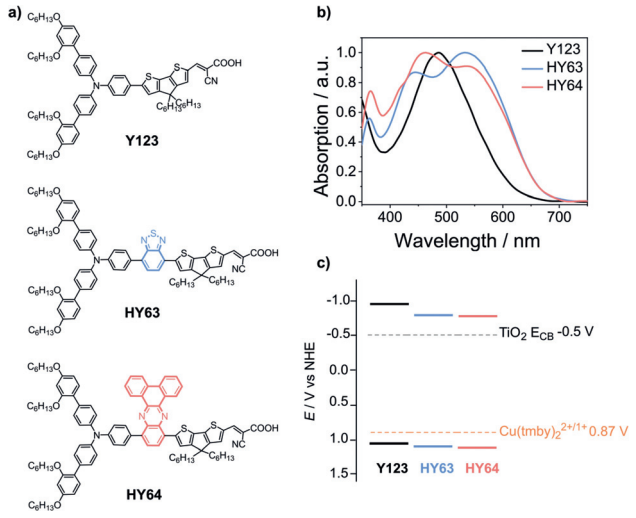

Figure 1. Tailoring sensitizers for extending spectral response. a) Chemical structures of dyes **HY63** and **HY64** and the reference dye **Y123**. b) Absorption spectra of dyes adsorbed on 2 μm-thick transparent TiO_2 films. c) LUMO and HOMO energy levels of sensitizers.

widely used benzothiadiazole (BT) as an auxiliary acceptor, even though **HY63** and **HY64** show similar energy levels and absorption onsets. Our in-depth kinetic studies reveal that the large and rigid PFQ structure is capable of retarding charge recombination, providing a new avenue to build up highly efficient panchromatic organic sensitizers.

The synthetic routes to the BT- and PFQ-based dyes **HY63** and **HY64** are depicted in Scheme S1 in the Supporting Information. The chemical structures of synthetic intermediates and target dyes have been fully confirmed by ^1H, ^{13}C NMR, and HRMS (Supporting Information, Figures S10–S23). The absorption spectra of dyes **Y123**, **HY63**, and **HY64** were first studied in CH_2Cl_2 solution (Supporting Information, Figure S1) as well as on mesoporous TiO_2 electrodes (Figure 1b), with detailed absorption parameters tabulated in Table 1. As shown in Figure 1b, the absorption thresholds of **HY63** and **HY64** are close to 780 nm, being redshifted by about 50 nm with respect to that of **Y123**. The molar extinction coefficients of both new dyes are also enhanced (8.46×10^4 and $6.56\times10^4\,M^{-1}cm^{-1}$ for **HY63** and **HY64**, respectively) compared to that of **Y123** ($5.24\times10^4\,M^{-1}cm^{-1}$). These features enable the extension of solar-light harvesting to longer wavelengths, which meets a prerequisite to improve the J_{SC} of DSSCs.

Table 1: Optical and electrochemical data for dyes **Y123**, **HY63** and **HY64**.

Dyes	λ_{max}[a] [nm]	ε[a] [$M^{-1}cm^{-1}$]	λ_{max}[b] [nm]	HOMO[c] [V]	$E_{0\text{-}0}$[d] [eV]	LUMO[e] [eV]
Y123	541	52400	486	1.07	2.01	−0.94
HY63	550	84600	532	1.12	1.91	−0.79
HY64	556	65600	538	1.14	1.91	−0.77

[a] Absorption peaks (λ_{max}) and corresponding molar extinction coefficients (ε) in CH_2Cl_2 solution. [b] Absorption peak measured on 2 μm-thick TiO_2 films. [c] HOMO levels estimated from the first formal oxidation potentials (versus NHE) in acetonitrile, with ferrocene as a reference and calibration. [d] Energy gap estimated from absorption thresholds of dye-grafted 2 μm-thick transparent TiO_2 films. [e] LUMO levels calculated according to LUMO = HOMO − $E_{0\text{-}0}$.

Cyclic voltammetry measurements (Supporting Information, Figure S2) confirmed that the HOMO levels of BT-based **HY63** and PFQ-based **HY64** are similar (1.12 V and 1.14 V vs. NHE, respectively), as shown in Figure 1c. The slight downshift in HOMO levels with respect to that of **Y123** (1.07 V vs. NHE) can be attributed to the incorporation of electron-withdrawing auxiliary acceptors. The deep HOMO levels facilitate dye regeneration by the Cu^I complexes, whose standard Nernst potential is located at 0.87 V vs. NHE,[6,26] while the significant downward shift in LUMO levels from **Y123** (−0.94 V) to **HY63** (−0.79 V) and **HY64** (−0.77 V) reduces the energy loss associated with the electron injection.

Standard DSSC devices based on **Y123**, **HY63**, and **HY64** were fabricated with a double-layer mesoporous TiO_2 photoanode (4 μm transparent layer plus 4 μm scattering layer), and used a solution of copper complex $[Cu(tmby)_2]^{2+/1+}(TFSI)_{2/1}$ (tmby, 4,4′,6,6′-tetramethyl-2,2′-bipyridine; TFSI, bis(trifluoromethanesulfonyl)imide) in acetonitrile as redox electrolyte and a PEDOT film on FTO conducting glass as counter electrode. We optimized the fabrication conditions for three dyes, and found that **HY63** dye requires chenodeoxycholic acid (CDCA) as co-adsorbent, while the best performance for **HY64** can be achieved without CDCA (Supporting Information, Tables S1 and S2). Figure 2a shows the corresponding photocurrent density–voltage (J–V) curves of such copper-based DSSCs, measured under standard AM1.5 G sunlight (100 mW cm^{-2}). Photovoltaic metrics derived from these curves are listed in Table 2. The reference device based on **Y123** shows a PCE of 10.3%, with a J_{SC} of 13.33 mA cm^{-2}, V_{OC} of 1028 mV, and FF of 74.9%, in good agreement with previous reports.[6,8] The

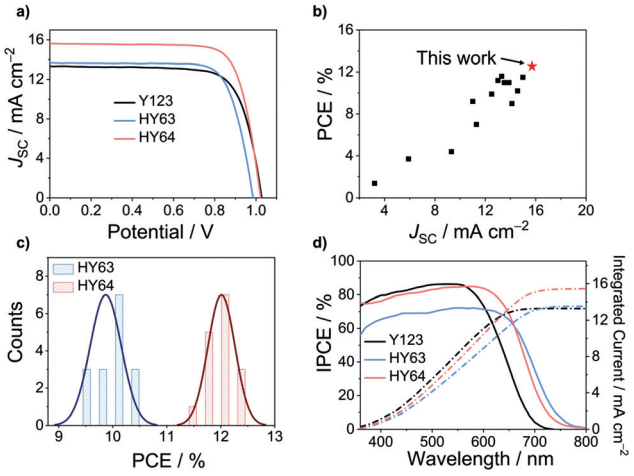

Figure 2. Comparison of device performances. a) J–V curves of optimized DSSCs based on dyes **Y123**, **HY63**, and **HY64**, with $[Cu(tmby)_2]^{2+/1+}$ as a redox shuttle, measured under AM1.5 G illumination. b) A summary of J_{SC} and PCE of reported high performing copper-based DSSCs with a single sensitizer. c) Histogram plots of solar-cell efficiencies (16 individual devices for sensitizers **HY63** and **HY64**). d) IPCE spectra and integrating current densities.

Table 2: Photovoltaic parameters of DSSCs based on dyes **Y123**, **HY63**, and **HY64**.

Dyes	J_{Cal}[a] [mA cm^{-2}]	J_{SC}[b] [mA cm^{-2}]	V_{OC} [mV]	*FF* [%]	PCE [%]
Y123	13.27	13.33	1028	74.9	10.3
HY63	13.55	13.71	986	76.4	10.3
HY64	15.40	15.76	1025	77.4	12.5

[a] J_{Cal} values calculated from IPCE spectra. [b] J_{SC} values measured under AM1.5 G simulated solar illumination (100 mW cm^{-2}).

PFQ-based dye **HY64** exhibits a striking improvement in J_{SC} (15.76 mA cm^{-2}), resulting in a much higher PCE of 12.5%, arising from the significant redshift in the absorption spectrum. To our knowledge, these are the highest J_{SC} and PCE values reported so far for DSSCs using a single sensitizer in combination with a $Cu^{II/I}$-based redox electrolyte (Figure 2b and Supporting Information, Table S4). By contrast, we did not observe the expected increase in J_{SC} with **HY63** containing benzothiadiazole as auxiliary acceptor, which showed a J_{SC} of 13.71 mA cm^{-2}, V_{OC} of 986 mV, and *FF* of 76.4%, corresponding to a PCE of 10.3%. We fabricated several batches of devices to compare the photovoltaic performances of **HY63** and **HY64**, demonstrating the good reproducibility of our results (Figure 2c and Supporting Information, Figure S3 and Table S3).

Figure 2d shows the IPCE spectra obtained with the three dyes along with the calculated J_{SC} values (J_{Cal} values) derived from the overlap IPCE integral with the AM1.5 G solar emission, which are in good agreement with the measured J_{SC}. The IPCE response for the **HY63**- and **HY64**-based devices is indeed extended to longer wavelengths by about 40–50 nm, resulting in a broader plateau than that of **Y123**. The plateau height of the **HY64**-based device is comparable to that of **Y123**, while the IPCE of **HY63** is lower with a smaller J_{SC} value. Figure S4 in the Supporting Information reveals that the light-harvesting spectra of **HY63** and **HY64** are very similar, indicating that the large difference in J_{SC} cannot be attributed to the optical absorption.

To scrutinize the reason for the superior performance of **HY64**, we first estimated the electron injection efficiency (η_{inj}) by measuring the steady state (Supporting Information, Figure S5) and transient photoluminescence (TRPL) spectra of dyes **HY63** and **HY64** adsorbed on mesoporous TiO_2 and Al_2O_3 films. The samples were immersed in $Cu(tmby)_2$-based electrolyte to mimic the conditions of operational DSSCs. The PL decays of dyes adsorbed on the mesoporous Al_2O_3 film (Figure 3a) provide amplitude-averaged lifetimes $\overline{\tau}(A)$ of 1.90 and 2.12 ns for **HY63** and **HY64**, respectively. The longer PL lifetime of dye **HY64** likely results from its more rigid PFQ-auxiliary acceptor skeleton. Upon adsorption onto TiO_2 film, the $\overline{\tau}(T)$ of **HY63** and **HY64** are shortened to 0.33 and 0.38 ns, respectively, reflecting quenching by electron injection into TiO_2. The η_{inj} estimated from the formula $\eta_{inj} = 1 - \overline{\tau}(T)/\overline{\tau}(A)$,[27–29] is 83% and 82% for **HY63** and **HY64**, respectively (Supporting Information, Table S5). The comparable electron injection efficiencies for both dyes are in line with their similar LUMO levels.

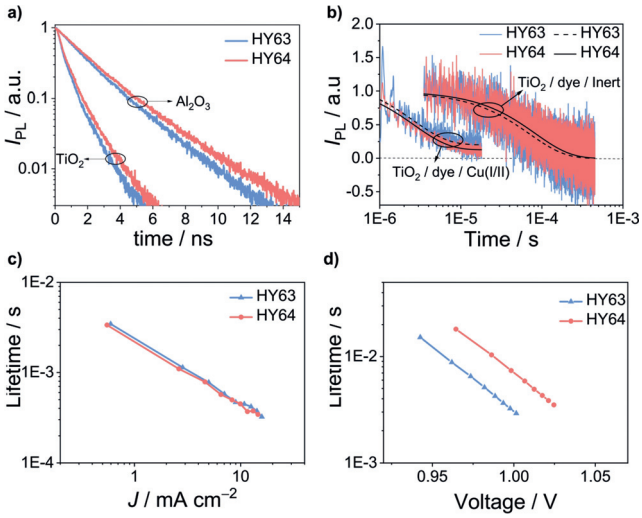

Figure 3. Interfacial charge dynamics study. a) Photoluminescence decay of **HY63**- and **HY64**-grafted mesoporous Al_2O_3 or TiO_2 films. Pump wavelength: 637 nm; probe wavelength: 770 nm. b) Flash photolysis measurement of dye-grafted TiO_2 films immersed in a $Cu(tmby)_2$-based redox electrolyte or an inert electrolyte. The solid lines are multiexponential fittings. Pump wavelength: 532 nm; probe wavelength, 840 nm. c) Charge transport lifetime and d) charge recombination lifetime measured by transient photocurrent/photovoltage techniques on complete devices.

We further used nanosecond laser flash photolysis measurements[30,31] to study the kinetics of the competing charge transfer reaction of the oxidized dye molecules (D^+) with either conduction band electrons in TiO_2 or Cu^I ions in the electrolyte (Figure 3b). When the dye-sensitized TiO_2 films are in contact with an inert electrolyte containing only 0.1 M lithium bis(trifluoromethanesulfonyl)imide (LiTFSI) and 0.4 M 1-butyl-1*H*-benzo[*d*]imidazole (NBB) in acetonitrile, the decay signals account for the back-electron-transfer from TiO_2 to D^+. The fitted carrier recombination lifetime ($\tau_{rec(dye)}$) values for this process are 71 and 83 μs for **HY63** and **HY64**, respectively. Upon contact with the $Cu(tmby)_2$-based electrolyte, the dye regeneration (lifetime ($\tau_{reg(dye)}$)) accelerates the signal decay by electron transfer from the Cu^I complex to D^+ as demonstrated by the corresponding values of 2.6 μs for **HY63** and 2.7 μs for **HY64**. Overall, the regeneration efficiency (η_{reg}) of the D^+ ($\eta_{reg} = k_{reg(dye)}/(k_{reg(dye)} + k_{rec(dye)})$, $k_{i(dye)} = 1/\tau_{i(dye)}$) is calculated as around 97% for both **HY63** and **HY64** (Supporting Information, Table S6). Therefore, dye regeneration does not explain the different IPCE plateaus.

Generally, the IPCE of DSSCs at a certain wavelength can be expressed as the product of light harvesting efficiency (LHE), electron injection efficiency (η_{inj}), dye regeneration efficiency (η_{reg}), and charge collection efficiency (η_{col}).[32–35] Since we have confirmed that the LHE, η_{inj}, and η_{reg} are very similar for dyes **HY63** and **HY64** in $Cu(tmby)_2$-electrolyte-based devices, the difference in their J_{SC} values should result from the effect of η_{col}. To gain further insight into the cause of this variation, we measured the charge transport and recombination lifetimes of complete devices by employing transient photocurrent and transient photovoltage techniques. Details

of the measurement methods are described in the Supporting Information. The apparent charge transport lifetimes (τ_{tans}) of **HY63**- and **HY64**-based devices under different light intensities are very close to each other, as shown in Figure 3c, while their recombination lifetimes (τ_{rec}) show large differences. As shown in Figure 3d, at a given V_{OC} modulated by bias light intensity, the τ_{rec} of the **HY64**-based device is two times longer than that of the **HY63**-based device, indicative of an enhanced η_{col} according to the relation, $\eta_{coll} = 1/(1+\tau_{trans}/\tau_{rec})$. Indeed, this can account for the observed increase in both IPCE plateau and J_{SC} values. Moreover, the resulting longer τ_{rec} for **HY64** also reflects a suppressed interfacial charge recombination, which can explain the approximately 40 mV higher V_{OC} of DSSCs based on **HY64** than that of **HY63**.

In order to further substantiate these results, we performed electrochemical impedance spectroscopy (EIS) measurements.[36,37] Figure 4a compares Nyquist (imaginary resistance versus real resistance) plots obtained with dyes **HY63** and **HY64** at a bias of 0.94 V. The large semicircle reflects the recapture of photo-injected electrons from the TiO_2 conduction band by the Cu^{II} complex at the TiO_2/electrolyte interface. Obviously, the semicircle radius of **HY64** exceeds that of **HY63**, indicating a larger recombination resistance (R_{CT}) at the TiO_2/dye/electrolyte interface. Figure 4b shows a plot of R_{CT} as a function of bias voltage. The R_{CT} of **HY64** is up to four times larger than that of **HY63**, further confirming suppressed recapture of the injected electrons by the Cu^{II} complex.

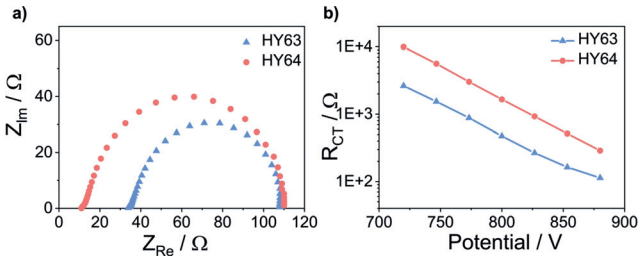

Figure 4. Charge transfer resistance study. a) Nyquist-type plots of **HY63**- and **HY64**-based solar cells from electrical impedance spectroscopy measurement by applying a bias of 0.94 V under white-light irradiation. b) Charge transfer resistance at the TiO_2/dye/electrolyte interfaces for devices fabricated with dyes **HY63** and **HY64** employing $[Cu(tmby)_2]^{2+/1+}$-based electrolytes.

Based on the above interfacial charge dynamics studies, we conclude that the inserted PFQ unit is preferable to the widely used BT in the judicious molecular design of long-wavelength-responsive DSSC sensitizers. It is capable of effectively supressing the loss in charge recombination, which is a key challenge in both metal-complex redox shuttles and low energy gap sensitizers. Figure S6 in the Supporting Information shows plots of the charge carrier collection efficiency (η_{coll}) defined by the equation $\eta_{coll} = 1/(1+\tau_{trans}/\tau_{rec})$, where τ_{trans} and τ_{rec} are the lifetimes for electron transport in the conduction band of mesoporous TiO_2 films (Supporting Information, Figure S7) and the interfacial recombination with Cu^{II} complex in the electrolyte, respectively. Obviously, the η_{coll} trends match closely those of IPCE plateaus in Figure 2d, confirming that the lower photocurrents observed with **HY63** arise from incomplete collection of the photogenerated charge carriers. This is further supported with a plot of the electron diffusion length (L_n) as a function of voltage (Supporting Information, Figure S8).The diffusion length of electrons for sensitizer **HY63** is too short to assure their quantitative capture, but for **HY64** L_n is about twice the TiO_2 film thickness, ascertaining near quantitative collection of photo-generated charge carriers.

From optical absorption measurements, we determined the loading of TiO_2 films with **HY63** and **H64** to be 8.51×10^{-8} and 7.05×10^{-8} mol cm^{-2} mm^{-1}, respectively. Hence the observed trends in the recombination lifetime and electron diffusion lengths might not originate from a variation of their surface coverage. We speculate that the large and rigid PFQ unit is less prone to association with $[Cu(tmby)_2]^{2+}$ electrolyte than BT, thus reducing the contact of Cu^{II} species in the electrolyte with the conduction band electrons in TiO_2. Therefore, the PFQ unit represents a promising building block for building up efficient long-wavelength-responsive sensitizers that are compatible with copper electrolytes.

As the copper redox shuttle can match well with a transparent PEDOT counter electrode, and dye **HY64** possesses quite high absorption coefficient, we tried to further remove the scattering TiO_2 layer to estimate the potential of this combination of dye, electrolyte, and counter electrode for semi-transparent photovoltaic applications, such as building-integrated photovoltaics (BIPVs). As shown in Figure 5a, the semi-transparent device exhibits excellent color rendering with color coordinates of (0.6597, 0.3184), and 43% transmittance of 690 nm light (Supporting Information, Figure S10). Notably, we achieved an unprecedented PCE of 11.2% for such semi-transparent DSSCs devices under full sunlight irradiation, with a comparable J_{SC} (14.80 mA cm^{-2}) to

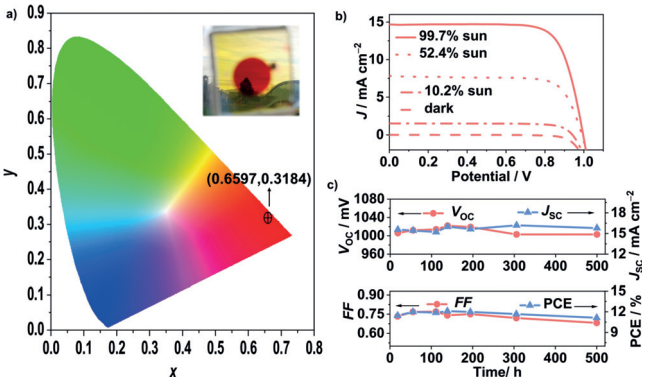

Figure 5. Semi-transparent devices with stability evaluation. a) Color coordinate of 4 μm-thick **HY64**-sensitized TiO_2 film in combination with $[Cu(tmby)_2]^{2+/1+}$-based electrolyte on the CIE 1931 *xy* chromaticity diagram. The inset shows a photograph of the real device. b) *J*–*V* curves for DSSCs fabricated with dye **HY64** adsorbed on the scattering layer of free TiO_2 film employing $[Cu(tmby)_2]^{2+/1+}$ as a redox shuttle measured under various light intensities. c) Evolution of V_{OC}, J_{SC}, *FF*, and PCE of dye **HY64**-based DSSCs measured under AM1.5 sunlight (100 mW cm^{-2}) during continuous light soaking at 60 °C for 500 h.

that of standard double TiO_2 layer-based devices (Figure 5b and Supporting Information, Table S7). To our knowledge, the efficiency value is the highest ever reported for semi-transparent DSSCs (Supporting Information, Figure S9 and Table S8). These preliminary results indicate that this prototype device is very promising for semi-transparent photovoltaics.

Finally, we evaluated the stability of the **HY64**-based copper electrolyte DSSC by keeping the device at open circuit under light soaking at 60 °C. The evolution of the PV metrics was recorded under full sun intensity at different time intervals. As shown in Figure 5c, the PCE retains 92 % of its peak value after 500 h solar light exposure, thereby confirming the high photostability of the prototype device.

In summary, we have demonstrated PFQ to be a promising auxiliary acceptor to extend the spectral response of organic dyes for improving the performance of copper-electrolyte-based DSSCs. The dye features a PFQ unit is superior to the BT unit, especially in reducing interfacial charge recombination. Without the requirement of any co-adsorbate, the PFQ-based D-A-π-A dye **HY64** achieves a J_{SC} of 15.76 mA cm^{-2} and a record PCE of 12.5 % in combination with a $Cu^{II/I}$-based redox electrolyte. which greatly exceeds that of the BT-based **HY63** as well as the reference sensitizer **Y123. HY64**-based DSSCs exhibit also a superior stability under continuous light soaking at 60 °C. Moreover, see-through devices achieve a PCE of 11.2 %, showing promise for semi-transparent photovoltaics. The PFQ building block enables the successful spectral extension and interfacial tailoring in copper-complex-based DSSCs, and further performance enhancement can be expected by molecular engineering on both the PFQ unit itself and the whole conjugated system.

Acknowledgements

This work was financially supported by NSFC/China (21788102, 21421004, 21905091, 21822504 and 21706070), Shanghai Municipal Science and Technology Major Project (2018SHZDZX03), Program of Introducing Talents of Discipline to Universities (B16017), Eastern Scholar (TP2016018), Science and Technology Commission of Shanghai Municipality (17ZR1407400), and China Association of Science and Technology (2017QNRC001), China Postdoctoral Science Foundation (No.2019M651418), and Fundamental Research Funds for the Central Universities (WJ1714007). H.Y.J. acknowledges China Scholarship Council (CSC) for a PhD study fellowship. M.G. acknowledges the financial support from the European Union's Horizon 2020 research and innovation program under grant agreement No. 826013. We thank Ladislav Kavan, from the J. Heyrovsky Institute of Physical Chemistry, who helped us to record the cyclic voltammograms during his time at EPFL.

Conflict of interest

The authors declare no conflict of interest.

Keywords:

[1] M. Freitag, Q. Daniel, M. Pazoki, K. Sveinbjörnsson, J. Zhang, L. Sun, A. Hagfeldt, G. Boschloo, *Energy Environ. Sci.* **2015**, *8*, 2634 – 2637.
[2] M. Freitag, F. Giordano, W. Yang, M. Pazoki, Y. Hao, B. Zietz, M. Grätzel, A. Hagfeldt, G. Boschloo, *J. Phys. Chem. C* **2016**, *120*, 9595 – 9603.
[3] Y. Cao, Y. Liu, S. M. Zakeeruddin, A. Hagfeldt, M. Grätzel, *Joule* **2018**, *2*, 1 – 10.
[4] Y. Bai, Q. Yu, N. Cai, Y. Wang, M. Zhang, P. Wang, *Chem. Commun.* **2011**, *47*, 4376 – 4378.
[5] M. Hu, J. Shen, Z. Yu, R. Liao, G. G. Gurzadyan, X. Yang, A. Hagfeldt, M. Wang, L. Sun, *ACS Appl. Mater. Interfaces* **2018**, *10*, 30409 – 30416.
[6] Y. Saygili, M. Söderberg, N. Pellet, F. Giordano, Y. Cao, A. B. Muñoz-García, S. M. Zakeeruddin, N. Vlachopoulos, M. Pavone, G. Boschloo, L. Kavan, J. Moser, M. Grätzel, A. Hagfeldt, M. Freitag, *J. Am. Chem. Soc.* **2016**, *138*, 15087 – 15096.
[7] Y. Liu, Y. Cao, W. Zhang, M. Stojanovic, M. I. Dar, P. Péchy, Y. Saygili, A. Hagfeldt, S. M. Zakeeruddin, M. Grätzel, *Angew. Chem. Int. Ed.* **2018**, *57*, 14125 – 14128; *Angew. Chem.* **2018**, *130*, 14321 – 14324.
[8] W. Zhang, Y. Wu, H. W. Bahng, Y. Cao, C. Yi, Y. Saygili, J. Luo, Y. Liu, L. Kavan, J. Moser, A. Hagfeldt, H. Tian, S. M. Zakeeruddin, W. Zhu, M. Grätzel, *Energy Environ. Sci.* **2018**, *11*, 1779 – 1787.
[9] A. Colombo, C. Dragonetti, M. Magni, D. Roberto, F. Demartin, S. Caramori, C. A. Bignozzi, *ACS Appl. Mater. Interfaces* **2014**, *6*, 13945 – 13955.
[10] M. Magni, R. Giannuzzi, A. Colombo, M. P. Cipolla, C. Dragonetti, S. Caramori, S. Carli, R. Grisorio, G. P. Suranna, C. A. Bignozzi, D. Roberto, M. Manca, *Inorg. Chem.* **2016**, *55*, 5245 – 5253.
[11] M. Karpacheva, F. J. Malzner, C. Wobill, A. Büttner, E. C. Constable, C. E. Housecroft, *Dyes Pigm.* **2018**, *156*, 410 – 416.
[12] P. Ferdowsi, Y. Saygili, S. M. Zakeeruddin, J. Mokhtari, M. Grätzel, A. Hagfeldt, L. Kavan, *Electrochim. Acta* **2018**, *265*, 194 – 201.
[13] Y. Cao, Y. Saygili, A. Ummadisingu, J. Teuscher, J. Luo, N. Pellet, F. Giordano, S. M. Zakeeruddin, J. E. Moser, M. Freitag, A. Hagfeldt, M. Grätzel, *Nat. Commun.* **2017**, *8*, 15390.
[14] J. Cong, D. Kinschel, Q. Daniel, M. Safdari, E. Gabrielsson, H. Chen, P. H. Svensson, L. Sunce, L. Kloo, *J. Mater. Chem. A* **2016**, *4*, 14550 – 14554.
[15] Y. Wu, W. Zhu, *Chem. Soc. Rev.* **2013**, *42*, 2039 – 2058.
[16] K. Pei, Y. Wu, W. Wu, Q. Zhang, B. Chen, H. Tian, W. Zhu, *Chem. Eur. J.* **2012**, *18*, 8190 – 8200.
[17] W. Zhu, Y. Wu, S. Wang, W. Li, X. Li, J. Chen, Z. Wang, H. Tian, *Adv. Funct. Mater.* **2011**, *21*, 756 – 763.
[18] Y. Xie, W. Wu, H. Zhu, J. Liu, W. Zhang, H. Tian, W. Zhu, *Chem. Sci.* **2016**, *7*, 544 – 549.
[19] Y. Wu, W. Zhu, S. M. Zakeeruddin, M. Grätzel, *ACS Appl. Mater. Interfaces* **2015**, *7*, 9307 – 9318.
[20] Y. Lu, Y. Cheng, J. Luo, W. Tang, S. Zhao, Q. Liu, Y. Xie, *Sci. China Chem.* **2019**, *62*, 494 – 502.
[21] P. Ferdowsi, Y. Saygili, W. Zhang, T. Edvinson, L. Kavan, J. Mokhtari, S. M. Zakeeruddin, M. Grätzel, A. Hagfeldt, *ChemSusChem* **2018**, *11*, 494 – 502.
[22] M. Freitag, J. Teuscher, Y. Saygili, X. Zhang, F. Giordano, P. Liska, J. Hua, S. M. Zakeeruddin, J. Moser, M. Grätzel, A. Hagfeldt, *Nat. Photonics* **2017**, *11*, 372 – 378.
[23] J. Kim, C. Song, H. Kim, I. Kang, W. Shin, M. Park, D. Hwang, *J. Polym. Sci. Part A* **2013**, *51*, 4136 – 4149.
[24] J. Yang, Y. Gao, T. Jiang, W. Liu, C. Liu, N. Lu, B. Li, J. Mei, Q. Peng, J. Hua, *Mater. Chem. Front.* **2017**, *1*, 1396 – 1405.

[25] T. Hu, L. Han, M. Xiao, X. Bao, T. Wang, M. Sun, R. Yang, *J. Mater. Chem. C* **2014**, *2*, 8047 – 8053.
[26] S. Hattori, Y. Wada, S. Yanagida, S. Fukuzumi, *J. Am. Chem. Soc.* **2005**, *127*, 9648 – 9654.
[27] Z. Yao, M. Zhang, R. Li, L. Yang, Y. Qiao, P. Wang, *Angew. Chem. Int. Ed.* **2015**, *54*, 5994 – 5998; *Angew. Chem.* **2015**, *127*, 6092 – 6096.
[28] Y. Ren, D. Sun, Y. Cao, H. N. Tsao, Y. Yuan, S. M. Zakeeruddin, P. Wang, M. Grätzel, *J. Am. Chem. Soc.* **2018**, *140*, 2405 – 2408.
[29] P. Wang, L. Yang, H. Wu, Y. Cao, J. Zhang, N. Xu, S. Chen, J. Decoppet, S. M. Zakeeruddin, M. Grätzel, *Joule* **2018**, *2*, 1 – 9.
[30] T. Daeneke, A. J. Mozer, Y. Uemura, S. Makuta, M. Fekete, Y. Tachibana, N. Koumura, U. Bach, L. Spiccia, *J. Am. Chem. Soc.* **2012**, *134*, 16925 – 16928.
[31] R. Shivanna, S. Shoaee, S. Dimitrov, S. K. Kandappa, S. Rajaram, J. R. Durrant, K. S. Narayan, *Energy Environ. Sci.* **2014**, *7*, 435 – 441.
[32] Z. Huang, X. Zang, T. Hua, L. Wang, H. Meier, D. Cao, *ACS Appl. Mater. Interfaces* **2015**, *7*, 20418 – 20429.
[33] K. Hara, T. Sato, R. Katoh, A. Furube, T. Yoshihara, M. Murai, M. Kurashige, S. Ito, A. Shinpo, S. Suga, H. Arakawa, *Adv. Funct. Mater.* **2005**, *15*, 246 – 252.
[34] Y. Zhang, X. Bao, M. Xiao, H. Tan, Q. Tao, Y. Wang, Y. Liu, R. Yang, W. Zhu, *J. Mater. Chem. A* **2015**, *3*, 886 – 893.
[35] J. Shi, Z. Chai, R. Tang, J. Hua, Q. Li, Z. Li, *Sci. China Chem.* **2015**, *58*, 1144 – 1151.
[36] C. Dong, W. Xiang, F. Huang, D. Fu, W. Huang, U. Bach, Y. Cheng, X. Li, L. Spiccia, *Angew. Chem. Int. Ed.* **2014**, *53*, 6933 – 6937; *Angew. Chem.* **2014**, *126*, 7053 – 7057.
[37] L. Zhang, X. Yang, W. Wang, G. G. Gurzadyan, J. Li, X. Li, J. An, Z. Yu, H. Wang, B. Cai, A. Hagfeldt, L. Sun, *ACS Energy Lett.* **2019**, *4*, 943 – 951.

Manuscript received: January 17, 2020
Accepted manuscript online: March 11, 2020
Version of record online: April 2, 2020

